Available online at www.sciencedirect.com

ScienceDirect

journal homepage: www.elsevier.com/locate/he

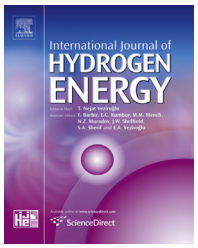

Computational fluid dynamics study of hydrogen generation by low temperature methane reforming in a membrane reactor

Syed A.M. Said [a,*,1], *David S.A. Simakov* [b,*,1], *Esmail M.A. Mokheimer* [a], *Mohamed A. Habib* [a], *Shakeel Ahmed* [c], *Mohammed Waseeuddin* [a], *Yuriy Román-Leshkov* [b,*]

[a] *Department of Mechanical Engineering, King Fahd University of Petroleum & Minerals, Dhahran 31261, Saudi Arabia*

[b] *Department of Chemical Engineering, Massachusetts Institute of Technology, Cambridge, MA 02139, USA*

[c] *Center for Refining and Petrochemicals, RI-King Fahd University of Petroleum & Minerals, Dhahran 31261, Saudi Arabia*

ARTICLE INFO

Article history:
Received 29 November 2014
Received in revised form
5 January 2015
Accepted 8 January 2015
Available online 28 January 2015

Keywords:
Hydrogen
Methane reforming
Membrane reactor
CFD model

ABSTRACT

Concentrated solar energy can be used to drive highly endothermic reactions, such as methane reforming. An attractive route is the parabolic trough technology, which is mature and relatively inexpensive but limited to temperatures below 600 °C, when methane conversions are low. However, high conversions are achievable if hydrogen is continuously removed from the reactive stream by a membrane selective to hydrogen. In this study, low temperature methane reforming in a membrane reactor is analyzed numerically by computational fluid dynamics over a wide range of operating parameters. Effects of temperature, steam-to-carbon ratio and space velocity on conversion, hydrogen recovery and carbon monoxide selectivity are specifically investigated. Our results show that concentration polarization can be significant. Below 500 °C the reactor performance is kinetically limited by the reforming reaction, while above this temperature hydrogen separation is a limiting factor. High hydrogen recovery is achievable even at high, industrially relevant space velocities. Importantly, hydrogen separation enhances water gas shift, reducing the concentration of carbon monoxide, the main source of coke formation at low temperatures.

* *Corresponding authors*. Tel.: +966 13 8603123; fax: +966 13 8602949.
E-mail addresses: samsaid@kfupm.edu.sa (S.A.M. Said), dsimakov@mit.edu (D.S.A. Simakov), yroman@mit.edu (Y. Román-Leshkov).

[1] These authors contributed equally.

http://dx.doi.org/10.1016/j.ijhydene.2015.01.024

Introduction

Most of the energy used worldwide is derived from fossil fuels by direct combustion, leading to excessive emission of carbon dioxide (CO_2) that contributes to global warming [1]. An alternative fuel is hydrogen (H_2) that have several advantages over fossil fuels, such as clean and more efficient combustion, and can be used for highly efficient and environmentally friendly electricity generation using fuel cells [2]. Hydrogen is also an important chemical feedstock with applications ranging from desulfurization, hydro treating, petroleum refining and production of chemicals [3]. Hydrogen is typically produced from hydrocarbons (mostly natural gas) by partial oxidation, autothermal reforming, dry reforming or steam reforming. Electrolysis can be used to generate H_2, but currently is too expensive to be deployed at large scale [4]. Among all methods mentioned above, steam methane (CH_4) reforming (SMR) is the cheapest and the most widely used method to produce H_2 on a commercial scale [5]. The use of steam as an oxidant is advantageous and relatively high H_2-to-carbon monoxide (CO) ratios obtainable by SMR are favorable for H_2 production [6].

The process of CH_4 reforming by steam can be described by the following reactions:

$$CH_4 + H_2O \rightleftarrows CO + 3H_2 \qquad \Delta H^{\circ}_{298} = 206\ \text{kJ/mol} \tag{1}$$

$$CO + H_2O \rightleftarrows CO_2 + H_2 \qquad \Delta H^{\circ}_{298} = -41\ \text{kJ/mol} \tag{2}$$

$$CH_4 + 2H_2O \rightleftarrows CO_2 + 4H_2 \qquad \Delta H^{\circ}_{298} = 165\ \text{kJ/mol} \tag{3}$$

Reaction (1) is SMR, reaction (2) is the water gas shift (WGS), and reaction (3) is the overall process, which is reversible (H_2 generation is favored at low pressures) and highly endothermic, requiring large heat inputs. In commercial installations, reformer tubes containing a Ni-based catalyst are heated by burning a fraction of natural gas (ca. 30%) and the CO produced is reacted with steam at lower temperatures in downstream WGS reactors catalyzed by Fe and Cu catalysts to produce more H_2. To prevent coking, high steam-to-carbon ratios are required for SMR (ca. 2–4), since running the process with stoichiometric feed composition leads to severe coking deactivation of Ni-based catalysts [7]. Nonetheless, Ni is inexpensive and features reasonably high catalytic activity. Platinum group metals have been also identified as excellent reforming catalysts but their implementation is hindered by the exceedingly high cost associated with current catalyst formulations that feature prohibitively high metal loadings (typically ranging from 1 to 5 wt%). Progress toward the use of platinum group metals for low temperature SMR was outlined in a recent review [8].

An attractive route to produce H_2, reduce CO_2 emissions, and save the otherwise combusted fraction of CH_4, is to use concentrated solar energy to provide the heat required for SMR [9–12]. This way, solar energy is used to upgrade the energy content of the hydrocarbon feedstock (e.g. natural gas) by converting it to a "solar" fuel consisting of a mixture of H_2 and CO (syngas) or H_2 (if additional steps of WGS and/or purification are implemented). The resulting "solar" H_2 can be used as a fuel for electricity generation in gas turbines or as a chemical feedstock. The high temperatures required for SMR historically limited the choice of a solar concentrator to solar dishes and central receivers [9–12] that have limited economic viability due to high capital costs. An alternative route is to use the mature and relatively inexpensive parabolic trough technology that can provide temperatures of ca. 400–600 °C when molten salts are used as heat carriers. In addition to high operational temperature, molten salts have other important advantages over conventional heat carriers such as steam and mineral oils, including low operational pressure, high heat capacity and density, high heat transfer coefficient and non-flammability. The solar heat is applied to the reformer indirectly, through the molten salt heat transfer fluid [13–16]. However, these temperatures are well below the operating temperature of conventional SMR reformers (850–950 °C). Therefore, to apply parabolic trough technology to SMR, it is critical to design an appropriate reforming system that can operate effectively at temperatures below 600 °C.

To overcome the thermodynamic limitations on CH_4 conversion imposed by low operating temperatures, membrane reformers can be implemented to continuously remove H_2 from the reactive stream and to shift the equilibrium towards the formation of products according to Le Chatelier's principle [17–21]. In a membrane reformer, complete CH_4 conversions are achievable well below 600 °C [22], thereby enabling the use of parabolic troughs for solar thermal SMR. The selective removal of H_2 can be effectively done by means of palladium (Pd)-based membranes, which are permeable exclusively to H_2 [23,24]. Though the cost of Pd is a prohibitive factor, recent developments provide a potential for mass production of Pd-based membranes at economically feasible costs [20]. Importantly, there is no additional energy investment for creating a pressure drop required to effectively separate H_2 by a Pd membrane (ca. 10 bar), since natural gas is already at pressures that exceed by far this requirement. In a recent experimental work reported by Patrascu and Sheintuch, SMR in a Pd membrane reformer designed specifically for solar thermal applications using molten salts as heat carriers was studied [25]. The reformer was packed with the Pt–Ni/CeO_2 catalyst supported on the SSiC ceramic foam (to improve heat transfer) and the membrane area was 175 cm^2. As a first step, the reformer was heated by an electrical furnace. Over 90% CH_4 conversion and over 80% H_2 recovery were achieved at 525 °C.

The separation characteristics of Pd-based membranes and their implementation in membrane reactors have been thoroughly investigated [20–24,26–30]. Goto et al. [28] studied H_2 permeation rate through a composite membrane with a Pd film coated on a porous ceramic tube and defined a numerical model based on the combined resistances of the Pd film and the composite support. Coroneo et al. [26,27] investigated mass transfer characteristics of Pd–Ag membrane H_2 separation modules experimentally and numerically using Computational Fluid Dynamics (CFD). Though porous ceramic membranes provide higher permeabilities, dense Pd membranes perform much better in SMR due to their exceptional selectivity. Uemiya et al. [17] compared the SMR performance of a supported Pd membrane and a porous Vycor glass membrane in a membrane reactor in a temperature range of 623–773 K. While the Pd membrane efficiently exceeded the equilibrium conversion, only a small change in equilibrium

was observed for porous Vycor glass. Simakov and Sheintuch provided experimental demonstration of the autothermal Pd membrane reformer and studied the effects of various parameters on the reformer performance [21,30]. It was shown that the reactor performance is strongly affected by the ratio of the feed rate to the maximal H_2 separation rate (membrane area and permeability).

Chibane and Brahim [18] studied a one dimensional model of a Pd membrane reactor for SMR, evaluating the reactor performance in terms of CH_4 conversion, H_2/CO ratio and H_2 recovery. The reactor performance was found to be optimal (nearly complete conversion and high H_2 recovery) for the temperature range of 580–600 °C, steam-to-methane ratio of 3, pressure range of 300–600 kPa and a sweep gas ratio of 3. In another simulation study conducted by Fernandes and Soares [19], it was shown that the membrane thickness is an important parameter in the membrane reactor performance and that the use of ultrathin membranes (μm scale) can significantly enhance methane conversions. Simakov and Sheintuch [22,29] defined a one dimensional non-isothermal model of the autothermal Pd membrane reformer and studied systematically the effects of various design and operation parameters on the reformer performance. The simulations mapped the acceptable domain of operation and the optimal set of operating parameters.

Although a significant amount of work has been done on the modeling of Pd membrane reactors, a simplified one-dimensional (1D) plug flow formulation is frequently applied, neglecting radial gradients [13,18,19,22,29]. Though such models can definitely describe the reactor performance approximately, more comprehensive formulation is required for more detailed analysis. It is highly desirable to account for radial gradients in simulations of membrane reformers. Since the driving force for H_2 separation is determined by the difference in H_2 partial pressures in the immediate vicinity of the membrane wall, the well-known phenomenon of concentration polarization will clearly limit the separation ability of the membrane and the overall performance of the membrane reformer in terms of CH_4 conversion and H_2 recovery. Though several two-dimensional (2D) studies of membrane reformers have been reported, they typically focus on a specific set or a narrow range of operating conditions and not always account for 2D velocity distribution which requires CFD modeling [31–33]. Also, there is a lack of systematic, generalized studies on the effects of industrially-relevant operating parameters, such as space velocity (i.e., reformer throughput).

Herein, we couple the detailed CFD modeling approach with an extended parametric study. We define a *2D CFD model* that describes a packed bed membrane reformer and analyze the reformer performance in SMR numerically. We focus on the low temperature regime achievable by parabolic trough solar collectors with molten salt as a heat transfer fluid (400–600 °C) and scan the reformer performance over a wide range of space velocities, including elevated, industrially-relevant values. Such extended parametric analysis, as opposed to a study with a fixed set of operating parameters, is very important for understanding design limits and optimization routes for practical implementation of a concept. We study the effects of space velocity, reformer temperature and feed steam-to-carbon ratio on the reformer performance in terms of CH_4 conversion, H_2 recovery, and H_2/CO ratio. Our findings show that the reformer performance can be *kinetically limited* (by the reforming reaction) or *mass transport limited* (by H_2 separation), depending on operating temperature and space velocity. High H_2 recovery is achievable even at elevated, industrially relevant space velocities. Importantly, H_2 separation enhances WGS, reducing the concentration of CO, which is the main source of coke formation at low temperatures.

Model formulation

Reformer configuration

Fig. 1 shows a schematic representation of the molten salt heated membrane reformer. The reformer size will be defined by the reformer most essential part, the H_2 separation membrane. The dimensions of the Pd membrane implemented in a recent experimental work [25], alongside with the corresponding dimensions suggested for the molten salt heated membrane reformer are listed in Table 1. In our numerical study, the axisymmetric tubular geometry of the membrane reformer is approximated by a 2D computational domain (Fig. 1c). The reformer geometry is defined by the reformer diameter (2R), the membrane diameter ($2R_M$) and the reformer length (L), or, for a fixed reformer length, by the aspect ratio 2R/L and the membrane surface-to-reformer volume ratio $S_M/V = 2R_M/R^2$. The inlet feed consists of CH_4 and H_2O (steam)

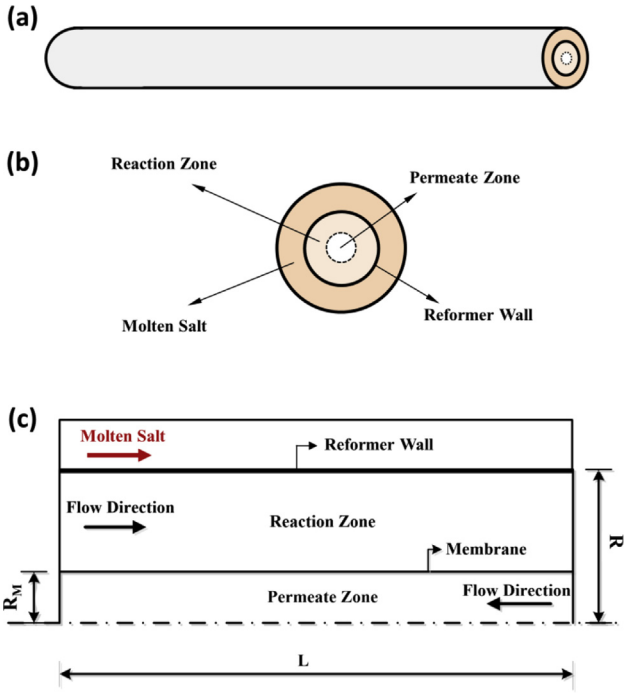

Fig. 1 – Schematic representation of the molten salt-heated membrane reformer (a) and its cross-sectional view (b); (c) A schematic of the 2D CFD computational domain (not to scale) representing a counter-current membrane reformer with tubular axisymmetric geometry.

Table 1 – Reformer dimensions.

D_M, mm	D_R, mm	D_{MS}, mm	L, mm
14	50	70	400

D and L denote diameter and length of the tubular membrane compartment and of the packed bed and molten salt shell compartments (Fig. 1). Subscripts M, R and MS stand for membrane, reaction zone and molten salt, respectively.

which are converted into H_2, CO and CO_2 over the catalytic packed bed. The produced H_2 permeates through the Pd membrane and removed by a sweep gas (e.g. steam). The reformer is operated in a counter-current mode (Fig. 1) to keep a high H_2 partial pressure difference along the axial dimension. Effects of the reformer temperature, steam-to-carbon molar ratio (S/C) and gas hourly space velocity (GHSV) on CH_4 conversion, H_2 recovery and CO selectivity (H_2/CO ratio) are investigated.

Model equations

The steady-state 2D CFD model employed in our study is based on the previously reported CFD models [26,27,34]. We assume a pseudo-homogeneous description of the catalytic bed [22,29], therefore the computational domain representing the catalytic packed bed is solved as a continuum. Details of the CFD formulation can be found elsewhere [35]. Briefly, model equations include continuity equation (Eq. (4)), momentum balance (Eq. (5)), energy balance (Eq. (6)) and species transport-reaction equation (Eq. (7)):

$$\nabla\cdot\left(\varepsilon\rho_f\vec{u}\right)=S_i \tag{4}$$

$$\nabla\cdot\left(\rho_f\vec{u}\vec{u}\right)=-\nabla p-\beta\vec{u}+\nabla\cdot\vec{\vec{\tau}}+\rho_f\vec{g} \tag{5}$$

$$\nabla\cdot\left(\rho_f\vec{u}h+\vec{u}p\right)=\nabla\cdot\left(k_e\nabla T-\sum_i h_i j_i+\vec{\vec{\tau}}\cdot\vec{u}\right)+(1-\varepsilon)\rho_c\sum_j R_j\Delta H_j \tag{6}$$

$$\nabla\cdot\left(\varepsilon\rho_f\vec{u}m_i\right)=\nabla\left(\rho_f D_{i,e}\nabla m_i\right)+(1-\varepsilon)\rho_c M_i\sum_j\alpha_{ij}R_j+S_i \tag{7}$$

In the equations above, β is the friction coefficient given by the following equation (we assume $\varepsilon=0.5$ and $d_p=3$ mm):

$$\beta=\frac{150\mu_f(1-\varepsilon)^2}{\varepsilon^3 d_p^2}+\frac{1.75(1-\varepsilon)\rho_f}{\varepsilon^3 d_p}|\vec{u}|\quad|\vec{u}|=\sqrt{u_r^2+u_z^2} \tag{8}$$

m_i is the mass fraction of species i, R_j is the reaction rate with a corresponding stoichiometric coefficient α_{ij}, ε is the void fraction of the packed bed and S_i is the source/sink term. For the reaction zone (Fig. 1c), which is packed with catalyst pellets, the model includes the reaction terms (R_j denotes the rate of a reaction j), the sink term (S_i) that accounts for H_2 removal by the membrane, and the friction term ($\beta\vec{u}$) to account for pressure losses along the packed bed. There is no catalyst in the molten salt and permeate zones ($\varepsilon=1$) and, therefore, there is no reaction there ($R_j=0$). There is no reaction or separation in the molten salt zone and, therefore, $m_i=0$ there.

Reaction rates are calculated using the commonly adopted SMR kinetics over the (MgO-promoted) Ni/Al_2O_3 catalyst [36,37] (p_i denotes the partial pressure of species i; a list of parameters can be found elsewhere [33]):

$$R_1=\frac{k_1}{p_{H_2}^{2.5}}\left(p_{CH_4}p_{H_2O}-\frac{p_{H_2}^3 p_{CO}}{K_{1,eq}}\right)\frac{1}{den^2} \tag{9a}$$

$$R_2=\frac{k_2}{p_{H_2}}\left(p_{CO}p_{H_2O}-\frac{p_{H_2}p_{CO_2}}{K_{2,eq}}\right)\frac{1}{den^2} \tag{9b}$$

$$R_3=\frac{k_3}{p_{H_2}^{3.5}}\left(p_{CH_4}p_{H_2O}^2-\frac{p_{H_2}p_{CO_2}}{K_{3,eq}}\right)\frac{1}{den^2} \tag{9c}$$

$$den=1+K_{CO}p_{CO}+K_{H_2}p_{H_2}+K_{CH_4}p_{CH_4}+\frac{K_{H_2O}p_{H_2O}}{p_{H_2}}$$

$$k_j=A_j\exp\left(\frac{-E_j}{R_gT}\right)\qquad K_i=B_i\exp\left(\frac{-\Delta H_i}{R_gT}\right)$$

The effectiveness factor was not taken into account in the kinetics equations since mass and heat transfer limitations are not expected for the small catalyst particle size ($d_p=3$ mm) we used in our simulations [22]. The source/sink term that accounts for mass flow of species across the membrane is given by Eq. (10), wherein the H_2 flux is given by Sievert's law, Eq. (11) ($p_{H_2,M}$ denotes the H_2 partial pressure in the permeate zone, $E_{H_2}=6.6$ kJ/mol, $A_{H_2}=0.4$ mol/(m^2 s bar$^{0.5}$) [22]). The term S_i is zero unless the computational cell is adjacent to the membrane, i.e. to the boundary between the reaction zone and the permeate zone of the computational domain (Fig. 1). Since the membrane is assumed to be permselective to H_2, $J_i=0$ (and thus $S_i=0$) for all species except for H_2.

$$S_i=\frac{A_M J_i M_i}{V} \tag{10}$$

$$J_{H_2}=A_{H_2}\exp\left(-\frac{E_{H_2}}{R_gT}\right)\left(p_{H_2}^{0.5}-p_{H_2,M}^{0.5}\right) \tag{11}$$

Numerical simulations were performed using the commercial CFD package Fluent 14.0 (ANSYS Inc., PA, USA) [35]. Pressure-velocity correction was done using the SIMPLE algorithm. Reaction rates and H_2 permeation were modeled by user-defined functions (C++) compiled and hooked in the Fluent software. Dependences of fluid density, viscosity, diffusivity, thermal conductivity and heat capacity on temperature, pressure and composition were accounted for using standard definitions built-in in the computation software. A small fraction of H_2 at the reaction zone entrance was used to prevent numerical problems that stem from the appearance of p_{H_2} in the denominator in Eq. (9).

Model validation

The accuracy of our model was verified versus experimental data reported in the literature [37]. The non-membrane reformer (without a Pd membrane, i.e. $S_{H_2}=0$) was simulated in a range of temperatures (isothermal operation was

assumed) and residence times reported in the experimental study which was used for model validation as a reference [37]. The inlet feed consisted of CH_4, H_2O and H_2, with S/C = 3 and $H_2/CH_4 = 1.25$, the porosity of the catalyst bed was set to 0.528 and the reformer exit pressure was 10 bar (as in the reference work [37]). Fractional CH_4 conversion was calculated by Eq. (12) using the reformer outlet molar flow rates obtained in the simulations. Fig. 2 shows the variation of fractional CH_4 conversion for different reforming temperatures over a range of space velocities. It can be seen that the simulated values are in a good agreement with the reported experimental values [37].

$$f = \frac{F_{CO} + F_{CO_2}}{F_{CO} + F_{CO_2} + F_{CH_4}} \tag{12}$$

Results and discussion

In all simulations, the dimensionless reformer geometry was defined by the reformer aspect ratio (2R/L = 0.125) and the membrane surface-to-reformer volume ratio ($S_M/V = 22.4\ m^{-1}$). Gas hourly space velocity (GHSV) is defined as the volumetric flow rate of CH_4 in the feed (defined at standard temperature and pressure) divided by the reformer volume (excluding the molten salt compartment):

$$GHSV = \frac{Q^{STP}_{CH_4,f}}{V} \tag{13}$$

Inlet feed consisted of (preheated to the reformer temperature) H_2O and CH_4 with a steam-to-carbon molar ratio of S/C = 1–3. Though our model does not account for carbon formation (which is expected to occur for S/C < 2 over Ni-based catalysts) we intentionally included the stoichiometric feed case (S/C = 1) in our analysis to evaluate the potential of the membrane reformer for low S/C operation. This is of particular importance for solar thermal reforming, wherein maximizing the reformer throughput is required to minimize capital cost investment. It should be mentioned here that the kinetic expressions used in the simulations were developed for MgO-promoted Ni/Al_2O_3, i.e. $Ni/MgAl_2O_4$, which is more stable against coking. Nevertheless, new catalysts, with superior stability against carbon deposition, should be developed for such applications. The pressure at the reaction zone outlet was fixed to P = 10 bar, whereas the pressure at the outlet of the permeation zone was $P_M = 1$ bar in all simulations. The counter-current sweep flow was used to keep high H_2 partial pressure difference along the reformer (Fig. 1a), with the sweep gas mass flow rate equivalent to that of the feed.

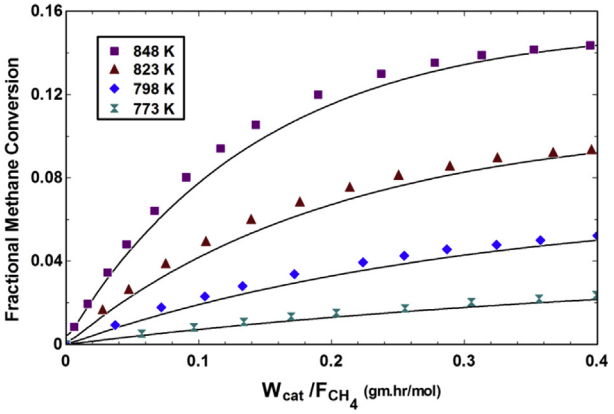

Fig. 2 – Model validation, comparing simulated variation of CH_4 conversion (lines) to experimental data (symbols, after [37]) for S/C = 3, P = 10 bar.

The reformer performance was evaluated by fractional methane conversion (Eq. (12)), H_2/CO ratio (accounting for combined H_2 flow at the outlet of the reaction and permeate zones) and H_2 recovery (the ratio of the molar rate of permeated H_2 (membrane outlet) to the feed CH_4 molar rate, Eq. (14)). The H_2/CO ratio is more useful evaluation parameter for applications wherein the total reformer outlet is used as a fuel (for gas turbine) or as a chemical feedstock, while H_2 recovery is more relevant for applications that require an extra-pure H_2 flow (e.g. fuel cells, hydrogenation etc.).

$$R_{H_2} = \frac{F_{H_2,M,out}}{F_{CH_4,f}} \tag{14}$$

Temperature distribution

We start with determining the molten salt velocity (u_{ms}), requiring that the rate of the sensible heat supply by the molten salt is equal to the rate of heat consumption by SMR ($\Delta H_{MSR+WGS}$ refers to the enthalpy of the combined process, Eq. (3)):

$$u_{ms} = \frac{F_{CH_4,f}\Delta H_{MSR+WGS}}{S_h \rho_{ms} C_{p,ms} T_{ms,f}} \tag{15}$$

where $F_{CH4,f}$ is the CH_4 molar feed rate, S_h is the reformer wall surface area, $T_{ms,f}$ is the molten salt feed temperature and ρ_{ms}, $C_{p,ms}$ are molten salt density and heat capacity (1899 kg/m^3 and 1495 J/(kg K) [38]). In order to achieve relatively uniform heating of the reformer, the heat should be supplied in large excess along the reformer tube. In this case the molten salt temperature profile is expected to be essentially flat, because the amount of heat transferred to the reformer compartment will contain only a small fraction of the total sensible heat stored in the molten salt [15].

Fig. 3 shows a representative temperature distribution within the reformer obtained with large excess of the molten salt supply, ten times higher than that calculated by Eq. (15), i.e. $10u_{ms}$. As it can be seen from Fig. 3, nearly uniform temperature distribution is obtained within the reaction zone of the reformer. The significantly lower temperature at the membrane interior entrance is due to the sweep gas (steam) entering at low temperature (above the boiling point of water). Supplying the molten salt in large excess in a practical situation is feasible, due to its high volumetric heat capacity. For example, for the case shown in Fig. 3 (GHSV = 1000 h^{-1}) supplying the heat carrier in 10-fold excess implies the molten salt flow of ca. 1 kg/h, which is definitely obtainable with the reformer dimensions listed in Table 1. In our further analysis we focus on concentration gradients and effects of operating parameters on the reformer performance in the low temperature range obtainable by solar parabolic trough

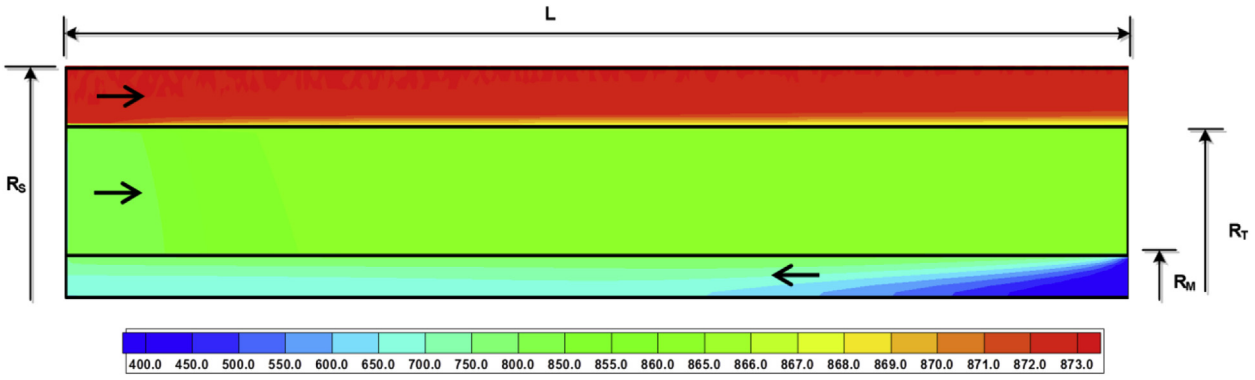

Fig. 3 – Temperature distribution within the reformer obtained with $T_{ms,f} = 873$ K, S/C = 3, GHSV = 1000 h^{-1}, P = 10 bar and $P_M = 1$ bar. Arrows show flow directions.

concentrators. We assume that the reformer reaction zone has uniform temperature distribution (as in Fig. 3) which implies that the molten salt is supplied in large excess.

Concentration polarization

Fig. 4 presents typical results, showing simulated contours of the H_2 mass fraction within the computation domain for S/C = 1, 3 and T = 773, 848 K. Since the flow of sweep gas is in the counter-current direction to the flow of reactants (see Fig. 1c), the highest values of the H_2 mass fraction in the permeate zone are observed at the inlet of the reaction zone, which is located at the same side as the exit for the sweep gas (flow directions are shown by arrows in Fig. 4). These plots clearly justify the use of the 2D model since strong radial gradients develop, leading to relatively low H_2 partial pressures at the membrane vicinity in the reaction zone. The buildup of the gradients is particularly pronounced in the beginning of the reaction zone in which the reforming reactions mostly take place. Since the driving force for H_2 separation is determined by the difference in H_2 partial pressures in the immediate vicinity of the membrane wall, concentration polarization limits the separation ability of the membrane and the overall performance of the membrane reformer in terms of CH_4 conversion and H_2 recovery.

Radial cuts of the 2D H_2 mass fraction distribution along the reactor length are shown in Fig. 5. Radial gradients are shown at four non-dimensional positions defined as x/L (x stands for the axial coordinate). The H_2 mass fraction decreases in both the reaction and permeate zones along the length of the reactor (in the direction of the reactants flow) as the H_2 formed by reforming reactions and WGS (Eqs. (1)–(3)) permeates through the membrane and accumulates in the permeate zone. The existence of concentration polarization is evidently seen from Fig. 5.

Methane conversion enhancement

Fig. 6 shows the simulated CH_4 conversion (Eq. (12)) at a fixed GHSV of 6000 h^{-1} and different S/C ratios, in the low temperature SMR range relevant to the solar parabolic trough technology. It can be seen that CH_4 conversions obtained in the membrane reformer exceeds by far those obtainable in the non-membrane reformer over the tested range of temperature and steam-to-carbon ratios (Fig. 6). The CH_4 conversion enhancement is due to the selective removal of H_2 by the Pd membrane that shifts the equilibrium towards H_2 generation (Eqs. (1)–(3)). This substantial increase in the CH_4 conversion compensates for low temperatures obtainable by solar parabolic troughs. For the given temperature, CH_4 conversion increases with steam-to-carbon ratio, both for membrane and non-membrane reactors (Fig. 6), which is dictated by equilibrium. Though it is expected to obtain higher conversions in a membrane reformer, the fact that such a significant enhancement is achievable at elevated space velocity (GHSV = 6000 h^{-1} in Fig. 6) is rather nontrivial and it emphasizes the potential of membrane reformers for high-throughput applications.

Three different steam-to-carbon ratios, S/C = 1, 2 and 3 were investigated. Though we aware of the tendency of the Ni catalyst to coke formation at S/C < 2 [7], S/C = 1 was included as a reference value that represents the ideal case with no coke formation (coking was not accounted for in our simulations). We note that CO is the main source of coking at relatively low temperatures, due to exothermic Boudouard coking and reverse gasification, while endothermic CH_4 cracking occurs at significantly higher temperatures. Interestingly, the results we present in next sections show that very low CO concentrations are obtained under certain operating conditions, thereby potentially allowing operating at low S/C ratios. Low CO concentrations can be attributed to low temperature regime of operation (WGS is exothermic, Eq. (2)) and to H_2 removal by the membrane.

Effect of temperature and steam-to-carbon ratio

Hydrogen recovery and H_2/CO ratio at different operating temperatures and steam-to-methane ratios are shown in Fig. 7. A general trend is observed showing that H_2 recovery increases for increasing temperature and S/C ratio (Fig. 7a). This increase is due to the faster reaction and separation kinetics at high temperatures (see Eqs. (9) and (11)) and an enhanced WGS reaction (Eq. (2)) in the presence of excess steam for high S/C ratios. Though the increase in H_2 recovery

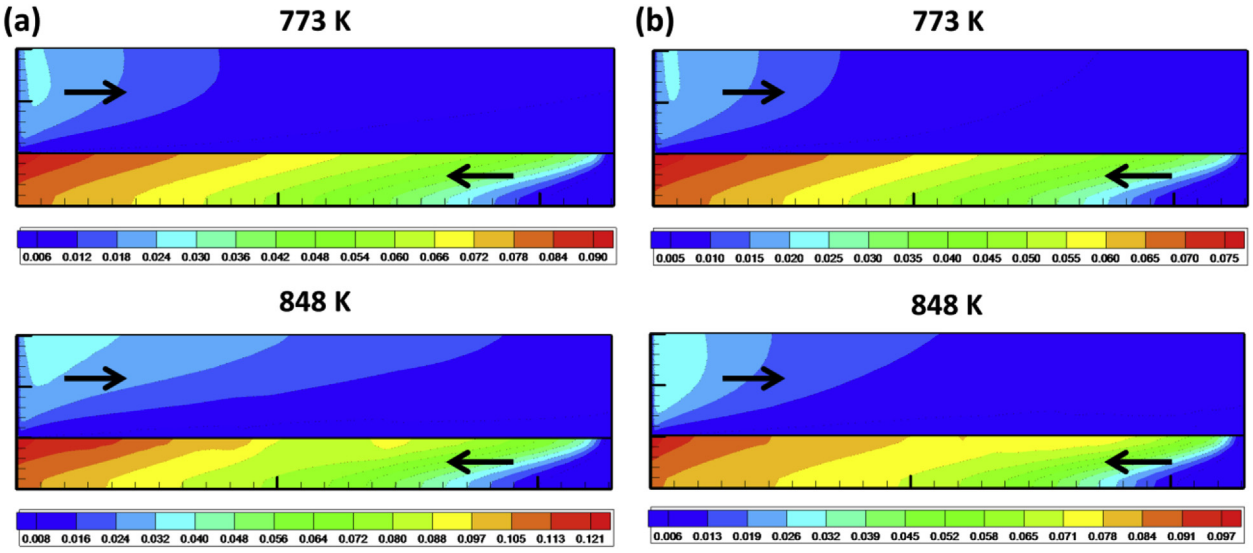

Fig. 4 – Simulated distributions of the H_2 mass fraction in the membrane reformer (not to scale) at T = 773 K and 848 K for S/C = 1 (a) and S/C = 3 (b); GHSV = 6000 h^{-1}, P = 10 bar and P_M = 1 bar. Arrows show flow directions.

is monotonic, three distinct ranges can be seen in Fig. 7a. There is a slow increase for T = 673–723 K followed by a sharp (about two-fold) improvement in the H_2 recovery for T = 723–773 K, while further increase in temperature results in only minor improvement again. Such trend clearly indicates the existence of (at least two) different limiting factors. The maximum H_2 recovery for isothermal operation is 4, as dictated by the reaction stoichiometry (Eq. (3)).

At very low temperatures (T < 720 K), the reformer performance is expected to be severely limited by the low activity of the Ni-based catalyst. The activation energy of the main reforming pathway is very high (E_1 = 240.1 kJ/mol, Eq. (9a) [37]), implying that the catalyst activity is very low below 720 K, but increases drastically for T ~ 770 K and above since the dependence of the reaction rate on temperature is highly nonlinear (Eq. (9)). This explains the two-fold increase in H_2 recovery for T = 720–770 K (Fig. 7a). The activation energy for H_2 separation is very low (E_{H_2} = 6.6 kJ/mol [22]) and is not expected to limit the reformer performance. The change in the slope of the H_2 recovery increase observed for T > 770 K (Fig. 7a) should be rather attributed to the lack of the membrane area [22] (this subject is discussed in more detail in Section 3.6), but could be also the result of the more pronounced concentration polarization (Figs. 4 and 5).

As expected, much higher H_2/CO ratios are obtained for higher steam-to-carbon ratio (Fig. 7b), as the WGS reaction extent is enhanced by excess steam. Note that very low CO concentrations are produced below 770 K. The decrease in H_2/CO ratio is observed with increasing operating temperatures, as it is expected from the exothermic nature of the WGS reaction. Comparing Fig. 7a and b shows that there is a tradeoff between high H_2 recovery and high H_2/CO ratio. Notably, T ~ 770 K provides an optimal value to obtain both a relatively high H_2 recovery (Fig. 7a) and an enhanced H_2/CO ratio (Fig. 7b). While high H_2 recovery is desirable for H_2 generation, low CO concentrations are preferable to prevent coking.

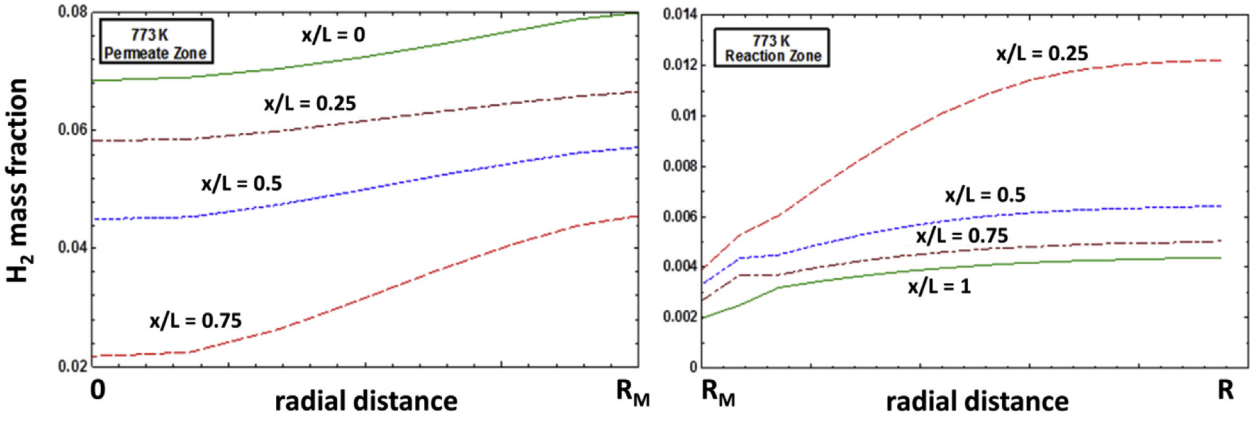

Fig. 5 – Simulated radial gradients of the H_2 mass fraction in the membrane interior (left panel) and the reformer reaction zone (right panel) at selected axial positions obtained at T = 773 K, S/C = 1 and GHSV = 6000 h^{-1}, P = 10 bar and P_M = 1 bar.

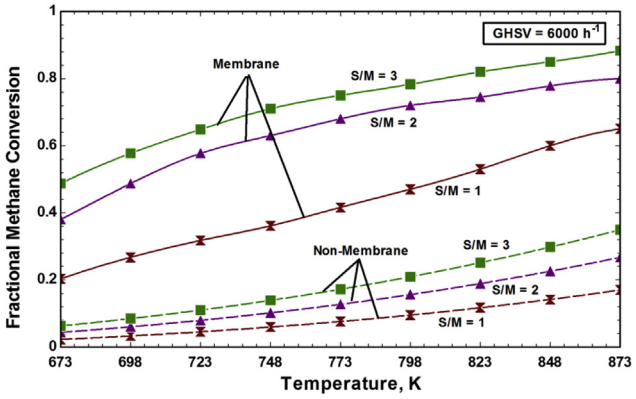

Fig. 6 – Fractional CH_4 conversion (Eq. (12)) vs. temperature for different S/C ratios (steam-to-methane fed, S/M) at GHSV = 6000 h^{-1}, P = 10 bar and P_M = 1 bar.

Effect of space velocity

Fig. 8 shows the impact of space velocity (GHSV) on CH_4 conversion, comparing the performance of the membrane and non-membrane reformers. GHSV is defined as the ratio of the CH_4 volumetric feed flow rate (calculated at standard conditions, i.e. STP) to the reactor volume, Eq. (13). The reformer was simulated for GHSVs ranging from 6000 h^{-1} to 15,000 h^{-1}, with S/C of 1 and 3, and operating temperatures of 773 K. Similarly to the results for a fixed GHSV shown before in Fig. 6, it is evident that a substantial increase in the CH_4 conversion is achieved by the membrane reactor for high GHSVs. Evaluating the performance of membrane reformers in a range of space velocities applicable to industrial conditions is of great importance to assess their potential for large-scale implementation. Importantly, although increasing GHSV leads to shorter contact times and lower CH_4 conversions, CH_4 conversion of ca. 50% is still achievable by the membrane reformer for GHSV = 15,000 h^{-1} and S/C = 3. It should be noted at this point that complete CH_4 conversions are not necessary required for applications that involve power generation using gas turbines using natural gas "upgraded" by solar energy. For such applications 50% conversion would be a very reasonable upgrade of the CH_4 heating value saving of ca. 10% of natural gas (as it can be easily calculated from heating values of corresponding gases) [39].

To determine the asymptotic limits of the reformer performance, we carried out numerical simulations in a wide range of space velocities, for GHSVs ranging from 500 h^{-1} to 100,000 h^{-1} (Fig. 9). We used low steam-to-carbon ratios (S/C = 1, 2), which are of particular importance for solar thermal reforming applications, wherein maximizing the reformer throughput is required to compensate for high capital cost investment. Generation of excess steam will consume a lot of solar energy, which can be otherwise converted into chemical energy. Simulations were run for temperatures of 673 K, 773 K and 848 K, signifying the temperature range obtainable by solar parabolic troughs.

As shown in Fig. 9, the equilibrium is approached as the GHSV tends to zero (infinite residence time). Membrane reactor equilibrium dictates nearly complete conversions for T > 770–820 K (depending on the S/C ratio) [22]. Another (kinetic) asymptote is approached as the GHSV tends to infinity (zero residence time). There is a sharp decrease in CH_4 conversion for GHSV >20,000 h^{-1}, while further increase in GHSV results in only minor further decrease of conversion, eventually attaining a plateau. In this regime, the reactor performance can be limited either kinetically (Ni catalyst activity) or by H_2 separation (membrane permeability and available membrane area), or both. For the reformer geometry analyzed in the present study, operation at GHSV <10,000 h^{-1} would be recommended; in order to further increase the operating GHSV either a more active catalyst, a more permeable membrane or a larger membrane area would be required [22].

Fig. 10 shows the variation of CH_4 conversion, H_2 recovery and H_2/CO ratio as a function of GHSV steam-to-carbon ratio of S/C = 1, 2 and 3, at T = 848 K. As it is dictated by the SMR-WGS equilibrium, higher CH_4 conversions are obtained for higher S/C ratios, due to the presence of excess steam in the reaction system. While steam-to-carbon ratios lower than S/C = 2 are not recommended due to catalyst coking deactivation issues (at least for Ni-based catalysts), excessively high S/C ratios demand more steam production, increasing the cost of the entire process unit. Thus, a tradeoff between the cost of the system and the catalyst activity and stability must be carefully evaluated depending upon the final application of the process.

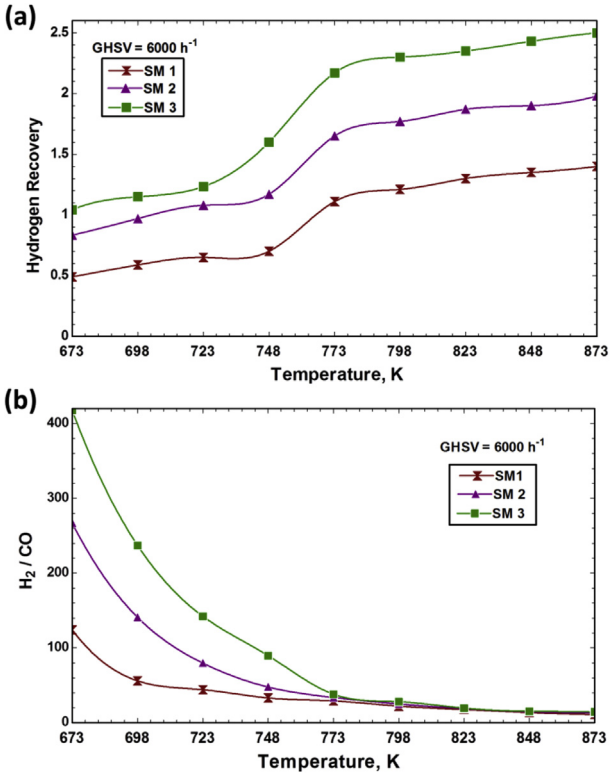

Fig. 7 – (a) H_2 recovery (Eq. (12)) and (b) H_2/CO ratio as a function of temperature for different S/C ratios (steam-to-methane fed, SM); GHSV = 6000 h^{-1}, P = 10 bar and P_M = 1 bar.

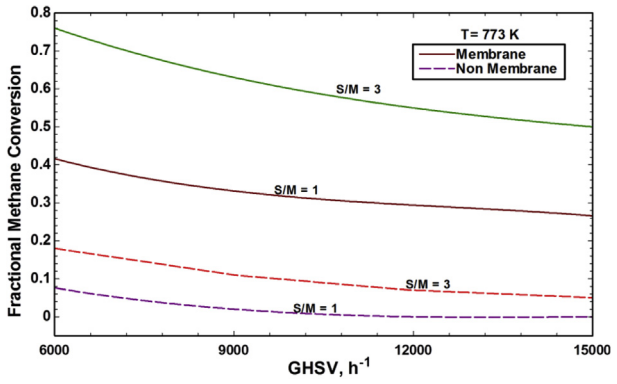

Fig. 8 – Comparison of performance of the membrane and non-membrane reformer in terms of CH_4 conversion (Eq. (10)) as a function of GHSV (Eq. (13)) for S/C = 1 and 3, T = 773 K, P = 10 bar and P_M = 1 bar.

Interestingly, although there is a significant drop in CH_4 conversion (Fig. 10a), the H_2 recovery values for S/C = 2 and 3 are still considerably high even for GHSV >20,000 h^{-1} (Fig. 10b). This observation demonstrates one of the important advantages of membrane reactors over conventional, non-membrane reformers: despite the drop of CH_4 conversion, H_2 separation by the membrane shifts the equilibrium of the WGS reaction towards production of more H_2 by converting CO to CO_2. Excess of steam that results from the low SMR conversion at high GHSV is in fact favorable for WGS. This is evident from the significant increase in the H_2/CO ratio at elevated space velocities (Fig. 10c). As a result, H_2 recovery of higher than 2 is achievable even at GHSV = 100,000 h^{-1} for S/C > 2. Therefore, though the introduction of the H_2 selective membrane requires a significant capital cost investment, membrane reformers could allow to operate within the regimes wherein the performance of a conventional reformer would be very poor.

Reformer performance limits

To generalize our findings, we provide herein a brief discussion on the performance limits of Pd membrane reformers in low temperature SMR. As it was shown in Section 3.4, H_2 recovery can be limited by multiple factors (Fig. 7a). It is evident that operation at T < 500 °C is disadvantageous because of the low activity (high activation energy) of the Ni catalyst. To estimate kinetic limits, it is useful to calculate Damköhler number for steam reforming reaction [22] (k_1 is from Eq. (9a) [37], $W_c = \rho_c(1-\varepsilon)V$, $F_{CH_4,f} = \rho_m Q^{STP}_{CH_4,f}$ and ρ_m stands for molar density of ideal gas):

$$Da_{SMR} = \frac{k_1}{F_{CH_4,f}/W_c} = \frac{A_1 \exp(-E_1/R_gT)\rho_c(1-\varepsilon)}{\rho_m GHSV/3600} \quad (16)$$

Substitution of relevant values into Eq. (16) shows that $Da_{SMR} \ll 1$ for T < 500 °C for the space velocity used in Fig. 7 (GHSV = 6000 h^{-1}), implying that the process is severely limited by the reaction kinetics. Typically, $Da_{SMR} > 10$ is required for good performance. As it can be seen from Eq. (16), this limitation will be even more severe at higher space velocities. The obvious way to improve the performance is to increase the temperature but, given that the upper limit is 600 °C (for the application considered here), more active catalysts would be eventually required to further increase the reformer throughput. Progress towards the development of alternative catalysts for low temperature SMR was outlined in a recent review [8].

Specifically for the membrane reformer, there is another useful dimensionless parameter, the membrane Péclet number (the ratio of the feed flow rate to the membrane separation rate) [22]:

$$Pe_M = \frac{F_{CH_4,f}}{S_M A_{H_2}\sqrt{P_{SR}}\exp(-E_{H_2}/R_gT)} = \frac{\rho_m GHSV/3600}{(S_M/V)A_{H_2}\sqrt{P_{SR}}\exp(-E_{H_2}/R_gT)} \quad (17)$$

For the parameters of Fig. 7, $Pe_M = 1.6–2$ depending on temperature, implying that the membrane reformer is slightly limited by H_2 separation ($Pe_M < 1$ is required for efficient H_2 recovery [22]). As the reformer throughput is increased (Figs. 9 and 10), Pe_M increases too, achieving $Pe_M \approx 5–7$ for GHSV = 20,000 h^{-1} and $Pe_M \approx 26–34$ for GHSV = 100,000 h^{-1}. Thus, a more permeable membrane (higher A_{H_2} and/or smaller E_{H_2} in Eq. (17)) or a larger membrane area-to-reformer volume ratio (S_M/V in Eq. (17)) would be required to improve the reformer performance, i.e. to obtain $Pe_M < 1$.

Below we provide a general guidance for the design of a membrane reformer. Calculating the dimensionless numbers mentioned above (Da_{SMR} and Pe_M) should be one of the very first steps. Following the selection of the required reformer throughput (a range of GHSV), the choice of catalyst should

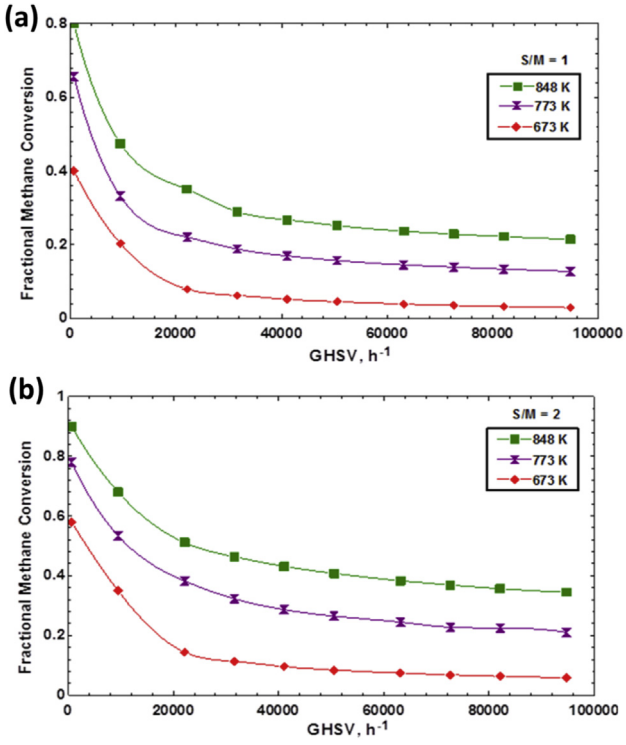

Fig. 9 – CH_4 conversion (Eq. (12)) as a function of GHSV (Eq. (13)) at various operating temperatures for S/C = 1 (a) and S/C = 2 (b).

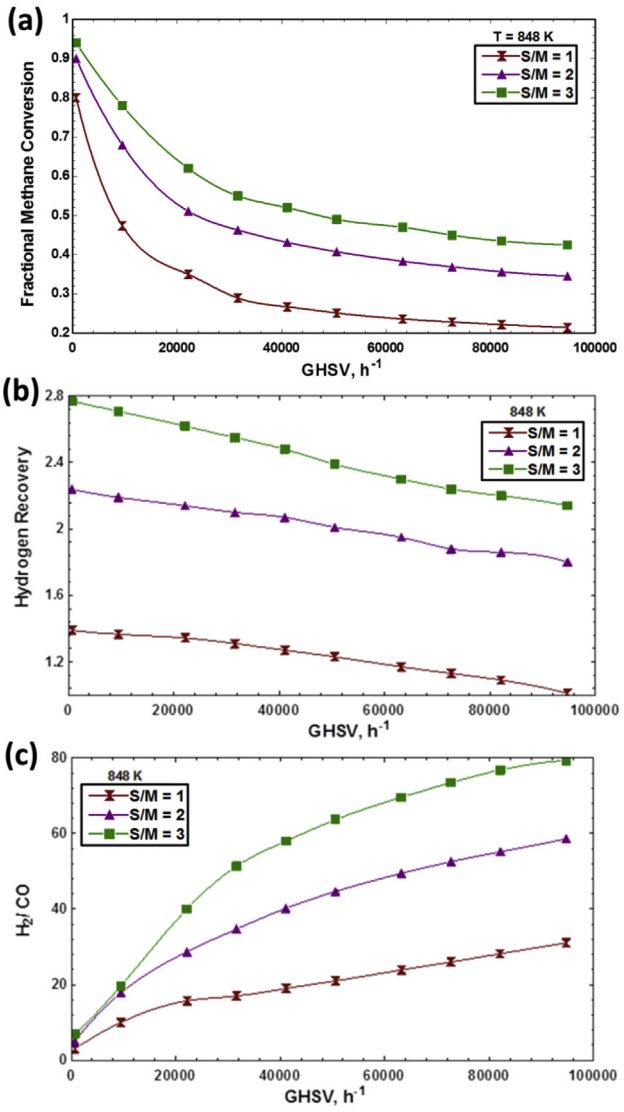

Fig. 10 – Variation of (a) CH_4 conversion (Eq. (10)), (b) H_2 recovery (Eq. (14)) and (c) H_2/CO ratio as a function of GHSV (Eq. 13) for different S/C ratios (steam-to-CH_4 fed, SM = 1, 2 and 3) at T = 848 K, P = 10 bar and P_M = 1 bar.

rely on its activity (A_1 and E_1 in Eq. (16)), to insure that $Da_{SMR} \gg 1$ in this range and for the particular temperature range selected. The selection of membrane should be based on its permeability (A_{H_2} and/or smaller E_{H_2} in Eq. (17)), while enough membrane area should be provided to keep $Pe_M \ll 1$.

Concluding remarks

Low temperature methane reforming in a palladium membrane reactor was analyzed numerically using computational fluid dynamics, in a specific temperature range relevant to solar thermal reforming applications using parabolic trough solar collectors. The simulation results show a significant buildup of radial gradients of hydrogen concentration and concentration polarization, justifying the use of the two-dimensional formulation. Effects of temperature, steam-to-carbon ratio and space velocity on conversion, hydrogen recovery and carbon monoxide selectivity were specifically investigated.

Our results show that, depending on the operating conditions, the membrane reformer performance can be kinetically limited, due to the low activity of the Ni-based catalyst, or limited by transport, due to hydrogen separation. Transport limitations can be intrinsic and global, due to limitations by membrane permeability to hydrogen or insufficient membrane area, or local, due to concentration polarization. These finding emphasize the importance of development of more active catalysts and more permeable membranes for low temperature methane reforming applications.

A significantly high hydrogen recovery is achievable in the membrane reformer at elevated, industrially relevant space velocities, even when moderate to low methane conversions are obtained. This effect was attributed to the enhancement of the water gas shift reaction by hydrogen separation. Importantly, the water gas shift enhancement also reduces the concentration of carbon monoxide, the main source of coke formation at low temperatures. Further work in underway, to study thermal effects in more detail and specifically to analyze the efficiency of the solar heat supply by a molten salt flow.

Acknowledgments

The authors highly appreciate and acknowledge the support of King Fahd University of Petroleum and Minerals through the research grant #R12-CE-10 offered by KFUPM-MIT Clean Water and Clean Energy Research Collaboration Center.

Nomenclature

A_j	pre-exponential factor of the rate coefficient of reaction j, units of k_j
A_{H_2}	membrane permeability to hydrogen, mol/(m^2 s bar$^{0.5}$)
A_M	membrane area, m^2
B_j	pre-exponential factor of the adsorption coefficient of species i, units of K_j
C_p	heat capacity, kJ/(kg K)
d_p	catalytic pellet diameter, m
$D_{i,e}$	effective diffusion coefficient of species i, m^2/s
E_{H_2}	membrane activation energy for hydrogen permeability, kJ/mol
E_j	activation energy of reaction j, kJ/mol
f	methane conversion
F_i	molar flow of species i, mol/s
$\vec{g}$	gravitational acceleration, m/s^2
$GHSV$	methane gas hourly space velocity, h^{-1}
h_i	specific enthalpy of species i, kJ/kg
ΔH_i	adsorption enthalpy change of species i, kJ/mol
J_{H_2}	hydrogen flux through the membrane, mol/(m^2 s)
k_e	effective thermal conductivity, kJ/(m s K)
k_j	rate constant of reaction j, units of Eq. (7)

K_i	adsorption constant of species i, units of Eq. (7)
$K_{j,eq}$	equilibrium constant of reaction j, units of Eq. (7)
L	reformer length, m
m_i	mass fraction of species i
M_i	molecular weight of species i, kg/mol
p	reactive mixture pressure, N/m^2
p_i	partial pressure of species i, bar
$p_{H_2,M}$	pressure at the permeate side, bar
P	pressure at the outlet of the reaction zone, bar
P_M	pressure at the outlet of the permeate zone, bar
$Q^{STP}_{CH_4,f}$	volumetric feed flow rate of methane (STP), Nm^3/h
R	reformer tube radius, m
R_M	membrane tube radius, m
R_j	rate of reaction j, mol/(kg s)
R_g	gas constant, kJ/(mol K)
R_{H_2}	hydrogen recovery
S_i	source term, kg/(m^3 s)
S/C	steam-to-carbon molar feed ratio
T	temperature, K
$\vec{u}$	fluid velocity, m/s
V	reformer volume, m^3
W_c	catalyst bed weight, kg

Greek letters

α_{ij}	stoichiometric coefficient of species i in reaction j
ε	catalyst bed porosity
μ_f	fluid viscosity, (N s)/m^2
ρ_c	catalyst bed density, kg/m^3
ρ_f	fluid density, kg/m^3
ρ_m	ideal gas density, mol/m^3
$\bar{\bar{\tau}}$	viscous stress tensor, N/m^2

REFERENCES

[1] Keller CF. Global warming 2007. An update to global warming: the balance of evidence and its policy implications. ScientificWorldJournal 2007;7:381–99.

[2] Balat M. Potential importance of hydrogen as a future solution to environmental and transportation problems. Int J Hydrogen Energy 2008;33:4013–29.

[3] Armor JN. The multiple roles for catalysis in the production of H_2. Appl Catal A 1999;176:159–76.

[4] Crabtree GW, Dresselhaus MS, Buchanan MV. The hydrogen economy. Phys Today 2004;57:39–45.

[5] Ewan BCR, Allen RWK. A figure of merit assessment of the routes to hydrogen. Int J Hydrogen Energy 2005;30:809–19.

[6] Holladay JD, Hu J, King DL, Wang Y. An overview of hydrogen production technologies. Catal Today 2009;139:244–60.

[7] Joensen F, Rostrup-Nielsen JR. Conversion of hydrocarbons and alcohols for fuel cells. J Power Sources 2002;105:195–201.

[8] Angeli SD, Monteleone G, Giaconia A, Lemonidou AA. State-of-the-art catalysts for CH_4 steam reforming at low temperature. Int J Hydrogen Energy 2014;39:1979–97.

[9] Piatkowski N, Wieckert C, Weimer AW, Steinfeld A. Solar-driven gasification of carbonaceous feedstock – a review. Energy Environ Sci 2011;4:73–82.

[10] Romero M, Steinfeld A. Concentrating solar thermal power and thermochemical fuels. Energy Environ Sci 2012;5:9234–45.

[11] Agrafiotis C, Hv Storch, Roeb M, Sattler C. Solar thermal reforming of methane feedstocks for hydrogen and syngas production – a review. Renew Sust Energ Rev 2014;29:656–82.

[12] Steinfeld A. Solar thermochemical production of hydrogen – a review. Sol Energy 2005;78:603–15.

[13] Giaconia A, Falco Md, Caputo G, Grena R, Tarquini P, Marrelli L. Solar steam reforming of natural gas for hydrogen production using molten salt heat carriers. AIChE J 2008;54:1932–44.

[14] Giaconia A, Turchetti L, Monteleone G, Morico B, Iaquaniello G, Shabtai K, et al. Development of a solar-powered, fuel-flexible compact steam reformer: the CoMETHy Project. Chem Eng Trans 2013;35:433–8.

[15] Falco MD, Giaconia A, Marrelli L, Tarquini P, Grena R, Caputo G. Enriched methane production using solar energy: an assessment of plant performance. Int J Hydrogen Energy 2009;34:98–109.

[16] Falco MD, Piemonte V. Solar enriched methane production by steam reforming process: reactor design. Int J Hydrogen Energy 2011;36:7759–62.

[17] Uemiya S, Sato N, Ando H, Matsuda T, Kikuchi E. Steam reforming of methane in a hydrogen-permeable membrane reactor. Appl Catal 1991;67:223–30.

[18] Chibane L, Djellouli B. Methane steam reforming reaction behaviour in a packed bed membrane reactor. Int J Chem Eng Appl 2011;2:147–56.

[19] Fernandes FAN, S Jr AB. Methane steam reforming modeling in a palladium membrane reactor. Fuel 2006;85:569–73.

[20] Sheintuch M, Simakov DSA. Alkanes dehydrogenation. In: Falco MD, Marrelli L, Iaquaniello G, editors. Membrane reactors for hydrogen production processes. New York: Springer-Verlag London Limited; 2011. p. 183–200.

[21] Simakov DSA, Sheintuch M. Demonstration of a scaled-down autothermal membrane methane reformer for hydrogen generation. Int J Hydrogen Energy 2009;34:8866–76.

[22] Simakov DSA, Sheintuch M. Model-based optimization of hydrogen generation by methane steam reforming in autothermal packed-bed membrane reformer. AIChE J 2011;57:525–41.

[23] Holleck GL. Diffusion and solubility of hydrogen in palladium and palladium-silver alloys. Phys Chem 1970;74:503–11.

[24] Yun S, Oyama ST. Correlations in palladium membranes for hydrogen separation: a review. J Memb Sci 2011;375:28–45.

[25] Patrascu M, Sheintuch M. On-site pure hydrogen production by methane steam reforming in high flux membrane reactor: experimental validation, model predictions and membrane inhibition. Chem Eng J 2015;262:862–74.

[26] Coroneo M, Montante G, Paglianti A. Numerical and experimental fluid-dynamic analysis to improve the mass transfer performances of Pd–Ag membrane modules for hydrogen purification. Ind Eng Chem Res 2010;49:9300–9.

[27] Coroneo M, Montante G, Baschetti MG, Paglianti A. CFD modelling of inorganic membrane modules for gas mixture separation. Chem Eng Sci 2009;64:1085–94.

[28] Goto S, Assabumrungrat S, Tagawa T, Praserthdam P. The effect of direction of hydrogen permeation on the rate through a composite palladium membrane. J Memb Sci 2000;175:19–24.

[29] Simakov DSA, Sheintuch M. Design of a thermally balanced membrane reformer for hydrogen production. AIChE J 2008;54:2735–50.

[30] Simakov DSA, Sheintuch M. Experimental optimization of an autonomous scaled-down methane membrane reformer for hydrogen generation. Ind Eng Chem Res 2010;49:1123–9.

[31] Kyriakides A-S, Ipsakis D, Voutetakis S, Papadopoulou S, Seferlis P. Modelling and simulation of a membrane reactor for the low temperature methane steam reforming. Chem Eng Trans 2013;35:109–14.

[32] Falco MD, Paola LD, Marrelli L, Nardella P. Simulation of large-scale membrane reformers by a two-dimensional model. Chem Eng J 2007;28:115–25.
[33] Rodríguez ML, Pedernera MN, Borio DO. Two dimensional modeling of a membrane reactor for ATR of methane. Catal Today 2012;193:137–44.
[34] Seo Y-S, Seo D-J, Seo Y-T, Yoon W-L. Investigation of the characteristics of a compact steam reformer integrated with a water-gas shift reactor. J Power Sources 2006;161:1208–16.
[35] FLUENT user's guide. Fluent Inc. http://www.fluent.com.
[36] Xu J, Froment GF. Methane steam reforming: II. Diffusional limitations and reactor simulation. AIChE J 1989;35:97–103.
[37] Xu J, Froment GF. Methane steam reforming, methanation and water–gas shift: 1. Intrinsic kinetics. AIChE J 1989;35:88–96.
[38] Kearney D, Herrmann U, Nava P, Kelly B, Mahoney R, Pacheco J, et al. Assessment of a molten salt heat transfer fluid in a parabolic trough solar field. J Sol Energy Eng 2003;125:170–6.
[39] Simakov DSA, et al. Solar thermal catalytic reforming of natural gas: a review on chemistry, catalysis and system design. Catal Sci Technol 2015. http://dx.doi.org/10.1039/c4cy01333f.